PCCP

PAPER

View Article Online
View Journal | View Issue

Cite this: *Phys. Chem. Chem. Phys.*, 2018, **20**, 10806

Theoretical kinetic study of the formic acid catalyzed Criegee intermediate isomerization: multistructural anharmonicity and atmospheric implications†

M. Monge-Palacios,*[a] Matti P. Rissanen,[b] Zhandong Wang[a] and S. Mani Sarathy[a]

Received 20th December 2017,
Accepted 29th January 2018

DOI: 10.1039/c7cp08538a

rsc.li/pccp

We performed a theoretical study on the double hydrogen shift isomerization reaction of a six carbon atom Criegee intermediate (C6-CI), catalyzed by formic acid (HCOOH), to produce vinylhydroperoxide (VHP), C6-CI + HCOOH → VHP + HCOOH. This Criegee intermediate can serve as a surrogate for larger CIs derived from important volatile organic compounds like monoterpenes, whose reactivity is not well understood and which are difficult to handle computationally. The reactant HCOOH exerts a pronounced catalytic effect on the studied reaction by lowering the barrier height, but the kinetic enhancement is hindered by the multistructural anharmonicity. First, the rigid ring-structure adopted by the saddle point to facilitate simultaneous transfer of two atoms does not allow the formation of as many conformers as those formed by the reactant C6-CI. And second, the flexible carbon chain of C6-CI facilitates the formation of stabilizing intramolecular C–H···O hydrogen bonds; this stabilizing effect is less pronounced in the saddle point structure due to its tightness and steric effects. Thus, the contribution of the reactant C6-CI conformers to the multistructural partition function is larger than that of the saddle point conformers. The resulting low multistructural anharmonicity factor partially cancels out the catalytic effect of the carboxylic acid, yielding in a moderately large rate coefficient, k(298 K) = 4.9 × 10^{-13} cm^3 $molecule^{-1}$ s^{-1}. We show that carboxylic acids may promote the conversion of stabilized Criegee intermediates into vinylhydroperoxides in the atmosphere, which generates OH radicals and leads to secondary organic aerosols, thereby affecting the oxidative capacity of the atmosphere and ultimately the climate.

I. Introduction

Criegee Intermediates[1] (CIs) are formed in the ozonolysis of unsaturated volatile organic compounds (VOCs), and their fate affects the composition of the troposphere.[2] CIs with an alkyl group in the *syn*-position can undergo unimolecular 1,4-hydrogen shift reactions to form vinylhydroperoxide (VHP), which decomposes to yield OH and vinoxy radicals. This isomerization can also be assisted by important atmospheric species like H_2O and organic acids. In addition, CIs can isomerize, leading to dioxirane (DIO),[3] and in the case of endocyclic alkenes, to secondary ozonide (SOZ) formation. The resulting species can further oxidize in the troposphere to form highly oxidized multifunctional compounds (HOMs),[4,5] which is currently considered as a major pathway for ambient secondary organic aerosol (SOA) production. In the atmosphere, SOA contribute to scattering and absorbing sunlight by growing cloud condensation nuclei, affecting the balance of solar radiation in the Earth.[6] The current mechanism assumes that the key step in forming HOMs is the unimolecular isomerization of CIs *via* 1,4-hydrogen shift to form VHP. A detailed understanding of the processes involved in HOM formation[4,5] is crucial to model the formation and evolution of SOA.[7–9] Despite their importance, the atmospheric reactivity of CIs is not fully understood, especially that of large CIs which have multiple potential product pathways available. Many of these large CIs are environmentally important biogenically derived species, thus being of special interest.

Previous studies have investigated the reactions of formic acid with simple CIs. For the reactions

$$CH_2OO + HCOOH/CH_3COOH \rightarrow Products \quad (R1)$$

[a] *King Abdullah University of Science and Technology, Clean Combustion Research Center, Thuwal 23955-6900, Saudi Arabia. E-mail: manuel.mongepalaciosm@kaust.edu.sa*

[b] *Department of Physics, University of Helsinki, P. O. Box 64, Helsinki, 00014, Finland*

† Electronic supplementary information (ESI) available. See DOI: 10.1039/c7cp08538a

and their analogues with CH_3CHOO, Welz *et al.*[10] measured rate coefficients of the order of 10^{-10} cm^3 $molecule^{-1}$ s^{-1} at 298 K for the overall CI loss, which quantifies the total CI decay without specifying the reaction pathways and products. They concluded that carboxylic acids may play a more important role in the loss process for CIs than previously assumed, and suggested that the rate coefficients of different sized CIs and carboxylic acids are of the same order. The catalytic effect of HCOOH was used by Liu *et al.*[11] to explain the results of their VUV photoionization experiments on the reaction

$$CH_3CHOO + DCOOD \rightarrow Products \quad (R2)$$

and those with $(CH_3)_2COO$ and CH_3CH_2CHOO. They measured a 50% yield of deuterated VHP and did not observe the formation of hydroperoxy ethyl formate, which results from the association of the CI and the acid. These results were attributed to the carboxylic acid, which enhances the formation of VHP. Due to their pronounced catalytic effect, carboxylic acids will promote the formation of VHPs in reactions like R2 and consume CIs,[12] especially in areas rich in these acids like forest, urban and marine areas,[13,14] also acting as sources of OH and SOA precursors. However, this scenario is currently uncertain for larger CIs, such as those formed in the ozonolysis of monoterpenes, for which detailed rate coefficient measurements are still lacking.

This work focuses on the 1,4-hydrogen shift isomerization reaction of the six carbon atom Criegee intermediate hexanal-6-oxide radical, hereafter C6-CI, catalysed by formic acid to form VHP:

$$C6\text{-}CI + HCOOH \rightarrow VHP + HCOOH \quad (R3)$$

C6-CI can serve as a prototype with a common structural unit to that of stabilized CIs (SCIs) formed from many abundant monoterpenes and other key biogenic VOCs. Thus, we chose a stabilized C6-CI and reaction (R3) as a model to obtain insight into the chemistry of the SCIs formed from large and relevant alkenes, which are difficult to handle computationally. Other alkenes like 6-nonenal are able to generate a stable form of C6-CI too.[15] The larger reactivity of CIs towards carboxylic acids compared to common atmospheric constituents like SO_2 and NO_2[16] makes the studied reaction important in the chemistry of the atmosphere; given the scarce data on large CIs, our study is useful to unravel their loss mechanism and fate, which are highly uncertain at the moment.

II. Computational methods: *ab initio* and rate coefficient calculations

The hybrid density functional ωB97X-D[17] and the 6-311+G(d,p)[18] basis set were used for the optimization and characterization of the stationary points of the reaction C6-CI + HCOOH → VHP + HCOOH, and to compute the minimum energy path, MEP, and the reaction valley. The energy of the stationary points was refined using the CCSD(T) coupled cluster method[19] with the same basis set. The electronic structure calculations were performed using the Gaussian-09 package.[20]

The MEP was calculated over the −2.0 to 2.0 Bohr range of the reaction coordinate s, using a step size of 0.04 Bohr in mass-scaled coordinates with a scaling mass equal to 1 amu, and the Hessian was evaluated at every step. The MEP was calculated using the Gaussrate-2016 code,[21] which is an interface between Gaussian-09[20] and Polyrate-2016.[22] With this information we calculated the ground-state vibrationally adiabatic potential energy curve, $V_a^G(s)$,

$$V_a^G(s) = V_{MEP}(s) + ZPE(s) \quad (1)$$

where $V_{MEP}(s)$ is the classical potential energy and $ZPE(s)$ is the zero-point energy at s.

The rate coefficient calculations for the reaction C6-CI + HCOOH → VHP + HCOOH were carried out using Polyrate 9.5;[23] MSTor code[24] was used to account for multistructural anharmonicity. We used the multistructural[25–27] canonical transition state theory with torsional anharmonicity and a coupled torsional potential, MS-T(C). The conformational rotational–vibrational partition function was calculated as

$$Q_{\text{con-rovib}}^{\text{MS-T(C)}} = \sum_{j=1}^{J} Q_{\text{rot},j} \exp(-\beta U_j) Q_j^{\text{HO}} \prod_{\eta=1}^{t} \bar{f}_{j,\eta} \quad (2)$$

The summation runs over the set of conformers J, $Q_{\text{rot},j}$ is the classical rotational partition function, and U_j is the energy defined with respect to that of the global minimum structure, set to $j = 1$. The factor β is $1/k_BT$. Q_j^{HO} is the normal-mode harmonic oscillator partition function, which is adjusted to introduce the torsional anharmonicity associated with the coupled torsion η by the term $\bar{f}_{j,\eta}$, and it is given by

$$Q_j^{\text{HO}} = \exp(-h\omega/2k_BT)[1 - \exp(-h\omega/k_BT)]^{-1} \quad (3)$$

The single-structural rotational–vibrational partition function for the conformer j is defined as

$$Q_{\text{con-rovib},j}^{\text{SS-T(C)}} = Q_{\text{rot},j} \exp(-\beta U_j) Q_j^{\text{HO}} \prod_{\eta=1}^{t} \bar{f}_{j,\eta} \quad (4)$$

The product term of eqn (2) and (4) is defined as

$$\prod_{\eta=1}^{t} \bar{f}_{j,\eta} = (2\pi\hbar\beta)^{t/2} \frac{\prod_{m=1}^{F} \omega_{j,m}}{\prod_{\bar{m}=1}^{F-t} \bar{\omega}_{j,\bar{m}}} \frac{\sqrt{\det \boldsymbol{D}_j}}{\prod_{\tau=1}^{t} M_{j,\tau}} \prod_{\eta=1}^{t} \exp\left(-\frac{\beta W_{j,\eta}^{(C)}}{2}\right) I_0\left(\frac{\beta W_{j,\eta}^{(C)}}{2}\right) \quad (5)$$

where $\bar{\omega}_{j,\bar{m}}$ and $\boldsymbol{D}_j$ are the torsion-projected normal mode frequencies and the Kilpatrick and Pitzer torsional moment of inertia matrices, respectively. $M_{j,\tau}$ are the local periodicity parameters for uncoupled torsions τ, and I_0 is a modified Bessel function.

Using eqn (2) and (4) we can define the multistructural torsional anharmonicity factor $F_X^{\text{MS-T(C)}}$ for the reactants ($F_R^{\text{MS-T(C)}}$) and saddle point ($F_{SP}^{\text{MS-T(C)}}$) as

$$F_X^{\text{MS-T(C)}} = Q_{\text{con-rovib},X}^{\text{MS-T(C)}} / Q_{\text{con-rovib},X,j=1}^{\text{SS-T(C)}} \quad (6)$$

and the multistructural torsional anharmonicity factor for the reaction

$$F^{\text{MS-T(C)}} = F_{\text{SP}}^{\text{MS-T(C)}}/F_{\text{R}}^{\text{MS-T(C)}} \quad (7)$$

The vibrational frequencies were scaled using a frequency scaling factor of 0.957[28] to obtain a more accurate zero point energy and $V_a^G(s)$ curve, and for a better description of the torsional anharmonicity. To account for the quantum effects on the reaction coordinate we used the small-curvature tunneling (SCT)[22] approach, obtaining the transmission coefficients κ^{SCT}. The final rate coefficient is calculated as

$$k^{\text{MS-T(C)/SCT}} = \kappa^{\text{SCT}} \Gamma \frac{k_B T}{h} \frac{Q_{\text{elec}}^{\neq} Q_{\text{con-rovib}}^{\text{MS-T(C)},\neq}}{\Phi_t Q_{\text{elec}}^{\text{R}} Q_{\text{con-rovib}}^{\text{MS-T(C)R}}} \exp(-\beta V^{\neq}) \quad (8)$$

where the superscripts $\neq$ and R stand for the conventional transition state and reactants (for instance, $Q_{\text{elec}}^{\text{R}} = Q_{\text{elec}}^{\text{C6-CI}} \cdot Q_{\text{elec}}^{\text{HCOOH}}$), respectively. The term Φ_t is the translational partition function per unit volume, which is calculated classically. The factor Γ is the recrossing transmission coefficient, given by the ratio of the CVT rate coefficient to the TST one. The terms κ^{SCT} and Γ are calculated using the global minimum structures and the harmonic oscillator approach.

For the reactant C6-CI, the torsions corresponding to the dihedral angles O1–C2–C4–C7 (τ_1), C2–C4–C7–C10 (τ_2), C4–C7–C10–C13 (τ_3), C7–C10–C13–C16 (τ_4) and C10–C13–C16–O18 (τ_5) (see Fig. S1 of the ESI† for the labelling) are strongly coupled; thus the Voronoi method implemented in MSTor[24] was used to estimate the periodicity parameters $M_{j,\tau}$ necessary to calculate the partition functions. The scheme NS : SC = 0 : 5 was used, where NS and SC stand for nearly separable and strongly coupled torsions. The torsion around the C16–O18 bond was not considered in the calculation of the multistructural partition function due to its large torsional barrier. To assign the values of the $M_{j,\tau}$ parameters for the reactant HCOOH we did not need the Voronoi method since there is only one dihedral angle τ, H–O–C–H, which interconverts the two conformers found for this reactant. Thus, $M_{j,\tau}$ was set to 2 for the conformers $j = 1$ and $j = 2$ of HCOOH. For the calculation of the multistructural partition function of the saddle point we used the same torsional space as that used for the reactant C6-CI (see Fig. S2 of the ESI† for the labelling). These torsions are strongly coupled in the saddle point too; thus the same scheme NS : SC = 0 : 5 was used for the Voronoi method.

III. Results and discussion

The zero point energy (ZPE) corrected potential energy profile depicting the consumption of C6-CI at the CCSD(T)/6-311+G(d,p)//ωB97X-D/6-311+G(d,p) level is shown in Fig. 1. The global minimum optimized structures of the stationary points of reaction (R3) are also shown. It should be noted that the unimolecular pathways to DIO, SOZ and VHP may not show the global minimum conformers for their corresponding saddle point and product stationary points; instead, the conformer that was optimized in our first optimization attempt is shown. Therefore, the barrier heights and the enthalpies of reaction of these pathways may be a little lower. This is also the case of the complex of the HCOOH-catalysed pathway to VHP.

The formation of SOZ from a thermalized CI is favoured kinetically and thermodynamically, with a barrier height and heat of reaction much lower than those of the VHP and DIO unimolecular pathways. However, in the presence of HCOOH the formation of VHP is efficiently catalysed and becomes barrier-less, with a submerged barrier at −5.0 kcal mol^{-1}. The process is highly exothermic, with an enthalpy of reaction of −23.5 kcal mol^{-1}. This could enhance VHP production among the other possible pathways of the reaction of C6-CI with HCOOH. We note that this conclusion is subject to the

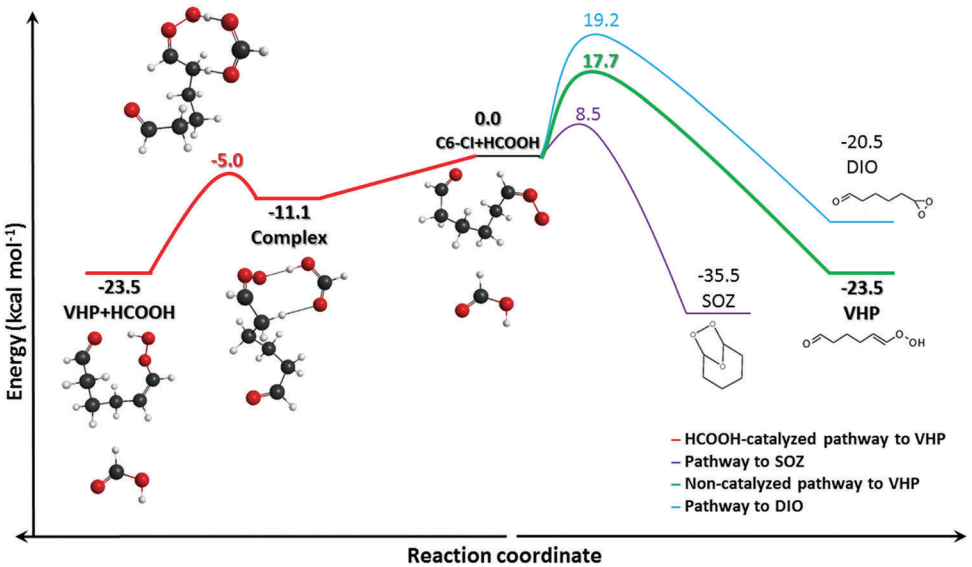

Fig. 1 Potential energy profiles (ZPE corrected) of the possible reaction pathways to the consumption of CI-C6 at the CCSD(T)/6-311+G(d,p)//ωB97X-D/6-311+G(d,p) level. Energy is defined with respect to the energy of the reactants (CI-C6/CI-C6 + HCOOH).

formation of SCIs with long enough lifetimes to react bimolecularily with carboxylic acids. For instance, while cyclohexene ozonolysis does not yield SCIs at atmospheric pressure,[29] larger and more atmospherically relevant VOCs do,[30] especially if the double bond attacked by ozone is in the exocyclic position.

Furthermore, we computed the rate coefficients for reaction (R3) in the temperature interval 230–2000 K using the multi-structural variational transition state theory, which accounts for the effect of the multiple conformers of the reactants and saddle point on the rate coefficient (multistructural anharmonicity). We calculated the rate coefficient over a broad temperature range to shed light on its temperature dependence. To do so, the search for the conformers was carried out by rotating the dihedral angles, exploring all the possible combinations. We found 394, 2 and 59 distinguishable structures for C6-CI, HCOOH, and the saddle point, respectively, which are convertible into each other by internal rotations of the dihedrals (the global minimum structures are shown in Fig. 1). The torsion around the C–O bond of C6-CI corresponds to the *syn*-CI ↔ *anti*-CI isomerization, whose barrier height was estimated to be ≈43 kcal mol^{-1}. The large internal energy of the CIs could potentially facilitate interconversion of their conformers; however, this will not be the case for the torsion around the C–O bond due its large barrier. Given that all the conformers of the saddle point are *syn*-conformers facilitating simultaneous transfer of two atoms, we believe that the *anti*-C6-CI conformers will not play a role in the studied reaction because they will not be likely converted into *syn*-C6-CI, and thus were not considered in the kinetic calculations. Although less prominent due to its lower stability, the formation of the *anti*-C6-CI conformer should also be expected in the ozonolysis process, as has been observed for other CIs.[30]

The harmonic vibrational frequencies of the global minimum structures of the stationary points of the studied reaction are listed in Table 1 at the ωB97X-D/6-311+G(d,p) level. Some key optimized bond distances are also shown. Important information can be inferred from the values of the O–O and C–O bond distances of C6-CI regarding its electronic character (that is, zwitterionic or diradical). It is known that a purely diradical character leads to an even distribution of the π electron density over the C–O–O group, resulting in similar C–O and O–O bond

Table 1 Harmonic vibrational frequencies and optimized geometric parameters of the global minimum structures of the stationary points of the reaction C6-CI + HCOOH → VHP + HCOOH at the ωB97X-D/6-311+G(d,p) level.[a] The point group is also shown

	Geometry[b]	Frequencies
C6-CI (C_1)		
r O(18)–O(19)	1.358	3216, 3137, 3121, 3104, 3065, 3060, 3053, 3051
r C(16)–O(18)	1.254	3025, 2921, 1839, 1613, 1503, 1490, 1477, 1446
		1425, 1408, 1396, 1384, 1383, 1356, 1307, 1279
		1232, 1202, 1126, 1103, 1079, 1024, 989, 969
		916, 913, 869, 818, 796, 700, 679, 659, 551, 440
		351, 331, 256, 181, 159, 144, 123, 71, 58
HCOOH (C_1)		
		3821, 3084, 1856, 1413, 1315, 1163, 1068, 684, 642
Complex (C_1)		
r O(22)–H(23)	1.003	3181, 3152, 3124, 3111, 3095, 3087, 3070, 3059
r H(23)–O(19)	1.626	3043, 3037, 3016, 2901, 1838, 1794, 1632, 1514
r O(24)–H(14)	2.130	1494, 1486, 1457, 1432, 1428, 1411, 1400, 1397
r H(14)–C(13)	1.098	1391, 1381, 1347, 1321, 1302, 1269, 1232, 1226
		1143, 1135, 1093, 1080, 1052, 1041, 1004, 972, 925
		891, 873, 826, 792, 747, 699, 689, 653, 533, 451
		350, 303, 277, 265, 238, 210, 183, 128, 120, 113
		98, 49, 32, 31, 25
Saddle point (C_1)		
r O(22)–H(23)	1.417	3135, 3134, 3121, 3116, 3107, 3074, 3062, 3052
r H(23)–O(19)	1.058	2992, 2930, 2205, 1864, 1821, 1683, 1662, 1506
r O(24)–H(14)	3.246	1503, 1491, 1465, 1428, 1420, 1400, 1394, 1386
r H(14)–C(13)	1.218	1384, 1364, 1343, 1326, 1297, 1283, 1220, 1209
		1155, 1129, 1109, 1087, 1076, 1053, 1045, 1011, 966
		927, 894, 831, 814, 765, 748, 668, 533, 498, 450
		378, 370, 326, 277, 243, 214, 167, 155, 122, 119
		98, 90, 57, 47, 340i
VHP (C_1)		
		3665, 3201, 3175, 3125, 3113, 3090, 3064, 3048
		3040, 2923, 1829, 1741, 1500, 1497, 1493, 1472
		1429, 1421, 1385, 1370, 1340, 1297, 1277, 1228
		1221, 1146, 1092, 1086, 1065, 1007, 983, 965, 956
		884, 835, 808, 770, 644, 594, 576, 513, 424, 383
		317, 258, 231, 206, 160, 130, 75, 47

[a] Distances are in angstroms, and frequencies in cm^{-1}. [b] See Fig. S1 and S2 of the ESI for the labelling.

distances.[31] This is not the case of C6-CI, which shows a shorter C–O bond, suggesting a double bond and thus a zwitterionic character.

The saddle point is characterized by a low imaginary frequency, 394 cm^{-1}. All the optimized conformers found for the stationary points of the studied reaction have been characterized as minima or saddle points by means of a vibrational frequency analysis.

The saddle point must adopt a constrained geometry with two collinear angles to allow a double hydrogen atom transfer reaction; this reduces its conformational space and may result in steric impediments, explaining the fewer conformers formed by the saddle point than by the reactant C6-CI. The flexible structure of C6-CI also forms more stable conformers by inducing more and stronger intramolecular C–H···O hydrogen bonds than those formed in the rigid structure of the saddle point. This effect is shown in the green upper panel of Fig. 2, with a potential energy distribution of the *syn*-C6-CI and saddle point conformers; the energy is shown on the green upper axis, and the values of the distributions are indicated in % on the bars. The potential energy profile of the reaction with the global minimum structures is also given (blue lower panel and axis). The energy values are reported relative to that of the global minimum and without the ZPE correction.

The energy distribution of the saddle point is much wider and peaks at higher energies. The low-energy conformers of C6-CI are folded, with the two terminal oxygen atoms pointing at the hydrogen atoms of the chain. In contrast, the high-energy conformers adopt a more linear structure or a folded one with the hydrogen atoms of the chain too close to each other. The same trend was observed in the saddle point, although with fewer and weaker C–H···O bonds due to its tight structure and steric effects. Thus, the stabilizing effect of the C–H···O bonds takes place to a larger extent in the reactant C6-CI than in the saddle point, which may help in increasing the barrier height and thus hindering the catalytic effect of the HCOOH. This effect could be more remarkable in large CIs due to their flexible carbon chain (see Section S1 of the ESI†). However, hydrogen bonds can also increase the free energy by reducing the entropy, and both energy contributions should be considered to get reliable conclusions. The free energy barrier for reaction (R3) is 6.8 kcal mol^{-1}.

The nature of the C–H···O hydrogen bonds has also been assessed by means of a natural bond orbital (NBO) analysis. These orbitals can be considered as one centre localized (lone pairs) or two centre localized (bonds) orbitals, that is, as in a Lewis structure, and they are obtained by the transformation of the canonical orbitals of the basis set using atomic natural and natural hybrid orbitals (ANO and NHO). In particular, we analysed the occupation of different antibonding molecular orbitals associated with the C–H bonds of the chain of the reactant C6-CI, σ_{C-H}^*, and their lone pair orbitals of the terminal oxygen atoms, n_{O-O} (peroxy group) and $n_{C=O}$ (carbonyl group).

For instance, the occupation numbers of the $\sigma_{C(7)-H(9)}^*$, $\sigma_{C(10)-H(12)}^*$, $\sigma_{C(4)-H(6)}^*$, and $\sigma_{C(13)-H(15)}^*$ orbitals of the conformer shown in Fig. S1(a) of the ESI† are 0.01067, 0.01091, 0.01165 and 0.01314, respectively, while those of the n_{O-O} and $n_{C=O}$ lone pair orbitals are slightly lower than 2.0, ranging from 1.9099 to 1.99216. This is an indication of electron density transfer from the n_{O-O} and $n_{C=O}$ lone pair orbitals (donors) to the σ_{C-H}^* orbitals (acceptors) and thus of C–H···O hydrogen bonds. This effect is even more pronounced in the C6-CI global minimum conformer, in which the occupancy of the $\sigma_{C(16)-H(17)}^*$ orbital becomes as large as 0.01576.

We also used the M05-2X[32] and M06-2X[33] density functional methods for the optimization and characterization of the

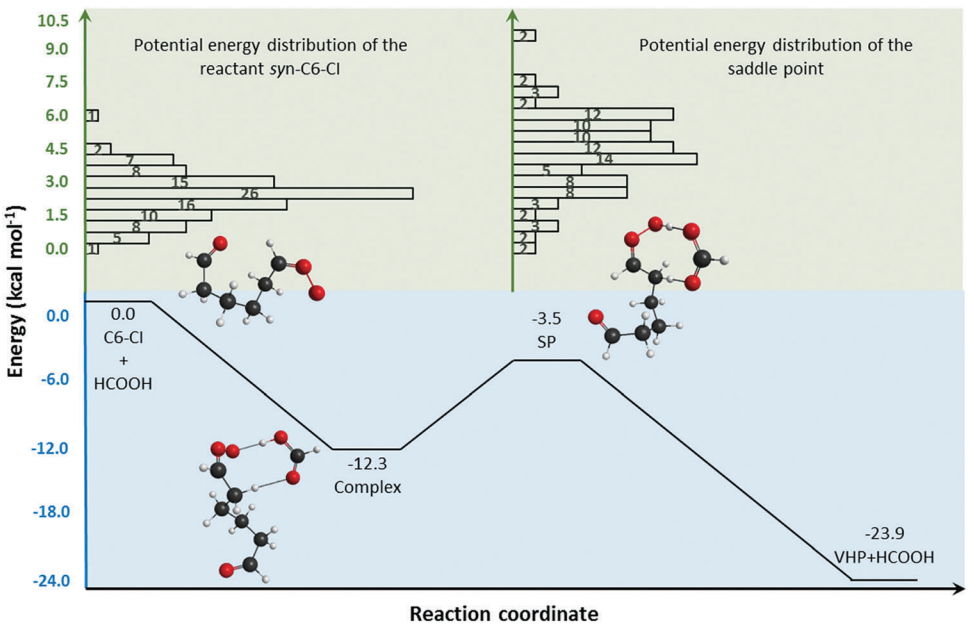

Fig. 2 Potential energy distribution (without the ZPE correction, units: % on bars) of the conformers of the reactant C6-CI and saddle point at the CCSD(T)/6-311+G(d,p)//ωB97X-D/6-311+G(d,p) level. Energy is defined relative to that of the global minimum.

stationary points of the titled reaction, which have also been proven to perform well in predicting barrier heights and describing non-covalent interactions such as hydrogen bonds. However, we were not able to optimize a few of the saddle point conformers found in our conformational search by using them, and these conformers would have been missed in the multi-structural treatment. For instance, the global minimum conformer of the saddle point found with the ωB97X-D method could not be optimized with the M05-2X and M06-2X methods, which instead derived that geometry to a different one, resulting in a barrier height of −3.4 kcal mol^{-1} (excluding the ZPE contribution) at the CCSD(T)/6-311+G(d,p)//M05-2X/6-311+G(d,p) and CCSD(T)/6-311+G(d,p)//M06-2X/6-311+G(d,p) levels. As for the reaction energy, these methods yielded values of −24.1 kcal mol^{-1} and −23.8 kcal mol^{-1}, respectively, in agreement with the value obtained with the CCSD(T)/6-311+G(d,p)//ωB97X-D/6-311+G(d,p) level (see Fig. 2 for comparison).

The differences in the potential energy distributions of the conformers of the reactant C6-CI and saddle point also have implications in the kinetics of the studied reaction by means of multistructural anharmonicity. The multistructural partition functions of the reactants and saddle point were calculated including torsional anharmonicity and a coupled torsional potential, MS-T(C). With this information, we calculated the multistructural anharmonicity factors for the aforementioned species and the total factor for the reaction: $F_{\text{C6-CI}}^{\text{MS-T(C)}}$, $F_{\text{HCOOH}}^{\text{MS-T(C)}}$, $F_{\text{SP}}^{\text{MS-T(C)}}$ and $F^{\text{MS-T(C)}}$. These factors are given at different temperatures in Table S1 and Fig. S3 of the ESI† (Section 2). The multistructural anharmonicity is more significant in the reactant C6-CI ($F_{\text{C6-CI}}^{\text{MS-T(C)}}$ (298 K) = 102.5) than in the saddle point ($F_{\text{SP}}^{\text{MS-T(C)}}$ (298 K) = 31.7), and negligible in HCOOH below 500 K ($F_{\text{HCOOH}}^{\text{MS-T(C)}}$ (298 K) = 1.0). As a result, the multistructural anharmonicity factor for the reaction C6-CI + HCOOH → VHP + HCOOH is lower than 1.0 in the whole temperature range ($F^{\text{MS-T(C)}}$ (298 K) = 0.3). These low values of $F^{\text{MS-T(C)}}$, and thus the hindering effect of the multistructural anharmonicity, should be attributed not only to the differences in the number of conformers of the reactant C6-CI and saddle point, but also to their different relative stability. The lower the energy of a conformer, the larger its contribution to the multistructural partition function. Due to the narrow energy distribution of the C6-CI conformers, even the higher-energy conformers contribute to the C6-CI multistructural partition function. The broad energy distribution of the saddle point makes many of its conformers play an unimportant role. These results are shown in Fig. S4 in the ESI.† Therefore, although the HCOOH exerts a remarkable catalytic effect by lowering the barrier height, the reactivity is also hindered by means of multistructural anharmonicity, thereby partially cancelling out the catalytic effect.

Using the multistructural anharmonicity factors we computed the rate coefficients $k^{\text{MS-T(C)}}$, which are tabulated in Table 2 and plotted in Fig. 3 as a function of temperature. For comparison purposes, the rate coefficients without multistructural anharmonicity (k^{CVT}) computed using the conventional canonical transition state theory with torsional anharmonicity are also given; these rate coefficients were calculated using eqn (8) with the single-structural rotational–vibrational partition functions given in eqn (4), instead of the multistructural ones defined in eqn (2). Quantum effects on the reaction coordinate are not important. The $k^{\text{MS-T(C)}}$ rate coefficients show a non-Arrhenius temperature dependence with a minimum at 1000 K, and a weak temperature dependence beyond 1000 K. Non-Arrhenius behavior has been reported for other reactions[34,35] with submerged barriers, resulting from a change in the activation energy from positive to negative as the temperature decreases. In the studied reaction that change occurs at 1000 K, and the rate coefficient increases at lower temperatures. The rate coefficients between 230 K and 320 K, which are more useful in atmospheric chemistry, were noted to obey the conventional Arrhenius equation and were fitted to the following expression:

$$k^{\text{MS-T(C)}}(T) = 9.30 \times 10^{6} T^{0.31} \exp\left(\frac{5070}{RT}\right) \qquad (9)$$

Comparing $k^{\text{MS-T(C)}}$ and k^{CVT}, it can be seen that the multistructural anharmonicity plays an important role; its hindering effect is more remarkable at temperatures near 350 K, where the factor $F^{\text{MS-T(C)}}$ shows a minimum ($F^{\text{MS-T(C)}}$ (350 K) = 0.3). Including this effect in the kinetic calculations can be critical for accurate predictions, but computationally expensive in large reactive systems.

Table 2 Rate coefficients (cm^3 molecule^{-1} s^{-1}) for the reaction C6-CI + HCOOH → VHP + HCOOH with ($k^{\text{MS-T(C)}}$) and without (k^{CVT}) multistructural anharmonicity

T (K)	$k^{\text{MS-T(C)}}/10^{-12}$	$k^{\text{CVT}}/10^{-12}$
230	5.568	16.664
240	3.535	10.752
250	2.338	7.204
260	1.598	4.993
270	1.130	3.571
280	0.819	2.615
290	0.611	1.965
298	0.491	1.588
310	0.362	1.179
320	0.287	0.940
350	0.157	0.517
400	0.073	0.240
500	0.028	0.089
600	0.017	0.049
800	0.011	0.028
1000	0.010	0.023
1200	0.011	0.023
1600	0.016	0.027
2000	0.023	0.036

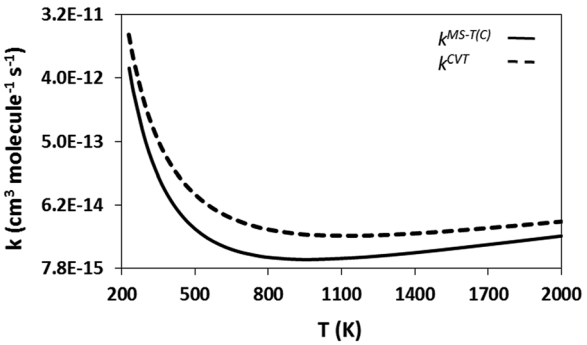

Fig. 3 Plots of $k^{\text{MS-T(C)}}$ and k^{CVT} (cm^3 molecule^{-1} s^{-1}) *versus* T (K).

We shall finalize by discussing the impact of the complex in the entry channel on the reaction kinetics; this complex lies on a well which is about −12.3 kcal mol^{-1} (see Fig. 2) below the reactants, and may lead to think of the studied reaction as a step-wise process with two consecutive steps:

$$\text{C6-CI} + \text{HCOOH} \rightleftharpoons \text{Complex} \rightarrow \text{VHP} + \text{HCOOH}$$

The first and second consecutive steps of the abovementioned scheme would be controlled by an outer and an inner transition state, respectively, with the inner transition state being the one considered in our kinetic calculations. However, the classical energy barrier to the second step, that is, the conversion of the complex into the final products, is 8.8 kcal mol^{-1} (see Fig. 2), while the first step in forming the complex from the reactants is barrier-less. Thus, we assumed that the barrier associated with the saddle point considered in our kinetic calculations represents the bottleneck of the overall process, and considered it as an elementary reaction C6-CI + HCOOH → VHP + HCOOH.

IV. Conclusions

We calculated the rate coefficients of the double hydrogen isomerization reaction of the Criegee intermediate hexanal-6-oxide radical, C6-CI, catalyzed by HCOOH, to produce vinylhydroperoxide (VHP), C6-CI + HCOOH → VHP + HCOOH. The multistructural anharmonicity turned out to have a hindering effect on the reactivity, which is attributed to the differences in the number and stability of the conformers formed by the reactants, C6-CI and HCOOH, and the saddle point of the reaction.

The result of the competition between the positive effect of the catalyzer HCOOH and the negative effect of the multistructural anharmonicity in the studied reaction is a moderately large rate coefficient with a non-Arrhenius temperature dependence. These findings lead us to the conclusion that reactions between SCIs and carboxylic acids may be an important intermediate step in the consumption and release of key biogenic emissions and VHPs, respectively, especially in areas rich in carboxylic acids and at low temperatures. These VHPs will generally undergo dissociation, releasing OH radicals in the troposphere, and thus enhance its oxidizing capacity. Upon dissociation, VHPs also release vinoxy radicals, whose oxidation is a common route to HOM species, which have recently been shown to be important atmospheric sources of SOA. It is well known that SOA have an important impact on climate and human health.

Thus, unraveling the fate and role of large VOCs and SCIs as SOA precursors is a key and challenging problem in atmospheric chemistry. Theoretically, the large number of heavy atoms present in those species makes the calculations an unfeasible task; experimentally, the determination of the rate coefficients for a specific reactive channel can be tremendously hard even for the smallest SCIs, and commonly only the rate of SCI consumption is determined. The studied reaction may be a useful prototype to model and understand the reactivity of carboxylic acids with larger SCIs produced in the ozonolysis of abundant VOCs such as monoterpenes, which share a common structural unit but are harder to assess computationally.

Conflicts of interest

There are no conflicts to declare.

Acknowledgements

This work was supported by the King Abdullah University of Science and Technology (KAUST), Office of Sponsored Research (OSR), under Award No. OSR-2016-CRG5-3022. MPR is grateful for the support from the Academy of Finland (project number 299574).

References

1 R. Criegee, Mechanism of Ozonolysis, *Angew. Chem., Int. Ed. Engl.*, 1975, **14**, 745–752.
2 D. Johnson and G. Marston, The Gas-phase Ozonolysis of Unsaturated Volatile Organic Compounds in the Troposphere, *Chem. Soc. Rev.*, 2008, **37**, 699–716.
3 J. Prousek, Chemistry of Criegee Intermediates, *J. Chem. Listy*, 2009, **103**, 271–276.
4 M. Ehn, J. A. Thornton, E. Kleist, M. Sipila, H. Junninen, I. Pullinen, M. Springer, F. Rubach, R. Tillmann, B. Lee, F. Lopez-Hilfiker, S. Andres, I. H. Acir, M. Rissanen, T. Jokinen, S. Schobesberger, J. Kangasluoma, J. Kontkanen, T. Nieminen, T. Kurten, L. B. Nielsen, S. Jorgensen, H. G. Kjaergaard, M. Canagaratna, M. D. Maso, T. Berndt, T. Petaja, A. Wahner, V. M. Kerminen, M. Kulmala, D. R. Worsnop, J. Wildt and T. F. Mentel, A Large Source of Low-volatility Secondary Organic Aerosol, *Nature*, 2014, **506**, 476–479.
5 T. F. Mentel, M. Springer, M. Ehn, E. Kleist, I. Pullinen, T. Kurten, M. Rissanen, A. Wahner and J. Wildt, Formation of Highly Oxidized Multifunctional Compounds: Autoxidation of Peroxy Radicals Formed in the Ozonolysis of Alkenes–Deduced from Structure–Product Relationships, *Atmos. Chem. Phys.*, 2015, **15**, 6745–6765.
6 J. H. Kroll, S. R. Sahay, J. G. Aderson, K. L. Demerjian and N. M. Donahue, Mechanism of HO_x Formation in the Gas-Phase Ozone-Alkene Reaction. 2. Prompt *versus* Thermal Dissociation of Carbonyl Oxides to Form OH, *J. Phys. Chem. A*, 2001, **105**, 4446–4457.
7 C. L. Heald, J. H. Kroll, J. L. Jimenez, K. S. Docherty, P. F. DeCarlo, A. C. Aiken, Q. Chen, S. T. Martin, D. K. Farmer and P. A. Artaxo, Simplified Description of the Evolution of Organic Aerosol Composition in the Atmosphere, *Geophys. Res. Lett.*, 2010, **37**, 1–5.
8 D. Johnson, S. R. Utembe, M. E. Jenkin, R. G. Derwent, G. D. Hayman, M. R. Alfarra, H. Coe and G. McFiggans, Simulating Regional Scale Secondary Organic Aerosol Formation during the TORCH 2003 Campaign in the Southern UK, *Atmos. Chem. Phys.*, 2006, **6**, 403–418.

9 D. Johnson, S. R. Utembe and M. E. Jenkin, Simulating the Detailed Chemical Composition of Secondary Organic Aerosol Formed on a Regional Scale During the TORCH 2003 Campaign in the Southern UK, *Atmos. Chem. Phys.*, 2006, **6**, 419–431.
10 O. Welz, A. J. Eskola, L. Sheps, B. Rotavera, J. D. Savee, A. M. Scheer, D. L. Osborn, D. Lowe, A. M. Booth, P. Xiao, M. A. H. Khan, C. J. Percival, D. E. Shallcross and C. A. Taatjes, Rate Coefficients of C1 and C2 Criegee Intermediate Reactions with Formic Acid and Acetic Acid Near the Collision Limit: Direct Kinetics Measurements and Atmospheric Implications, *Angew. Chem., Int. Ed.*, 2014, **53**, 4547–4550.
11 F. Liu, Y. Fang, M. Kumar, W. H. Thompson and M. I. Lester, Direct Observation of Vinyl Hydroperoxide, *Phys. Chem. Chem. Phys.*, 2015, **17**, 20490–20494.
12 H. J. Tobias and P. J. Ziemann, Kinetics of the Gas-Phase Reactions of Alcohols, Aldehydes, Carboxylic Acids, and Water with the C13 Stabilized Criegee Intermediates Formed from Ozonolysis of 1-Tetradecene, *J. Phys. Chem. A*, 2001, **105**, 6129–6135.
13 E. Sanhueza, L. Figueroa and M. Santana, Atmospheric Formic and Acetic Acids in Venezuela, *Atmos. Environ.*, 1996, **30**, 1861–1873.
14 K. Granby, C. S. Christensen and C. Lohse, Urban and Semirural Observations of Carboxylic Acids and Carbonyls, *Atmos. Environ.*, 1997, **31**, 1403–1415.
15 M. P. Rissanen, T. Kurten, M. Sipila, J. A. Thornton, J. Kangasluoma, N. Sarnela, H. Junninen, S. Jørgensen, S. Schallhart, M. K. Kajos, R. Taipale, M. Springer, T. F. Mentel, T. Ruuskanen, T. Petaja, D. R. Worsnop, H. G. Kjaergaard and M. Ehn, *J. Am. Chem. Soc.*, 2014, **136**, 15596—15606.
16 O. Welz, J. D. Savee, D. L. Osborn, S. S. Vasu, C. J. Percival, D. E. Shallcross and C. A. Taatjes, Direct Kinetic Measurements of Criegee Intermediate (CH_2OO) formed by Reaction of CH_2I with O_2, *Science*, 2012, **335**, 204–207.
17 J. D. Chai and M. Head-Gordon, Long-range Corrected Hybrid Density Functionals with Damped Atom-atom Dispersion Corrections, *Phys. Chem. Chem. Phys.*, 2008, **10**, 6615–6620.
18 R. J. Bartlett, Coupled-cluster Approach to Molecular Structure and Spectra: a Step toward Predictive Quantum Chemistry, *J. Phys. Chem.*, 1989, **93**, 1697–1708.
19 R. Krishnan, J. S. Binkley, R. Seeger and J. A. Pople, Self-consistent Molecular Orbital Methods. XX. A Basis Set for Correlated Wave Functions, *J. Chem. Phys.*, 1980, **72**, 650–700.
20 M. J. Frisch, G. W. Trucks, H. B. Schlegel, G. E. Scuseria, M. A. Robb, J. R. Cheeseman, G. Scalmani, V. Barone, B. Mennucci, G. A. Petersson, H. Nakatsuji, M. Caricato, X. Li, H. P. Hratchian, A. F. Izmaylov, J. Bloino, G. Zheng, J. L. Sonnenberg, M. Hada, M. Ehara, K. Toyota, R. Fukuda, J. Hasegawa, M. Ishida, T. Nakajima, Y. Honda, O. Kitao, H. Nakai, T. Vreven, J. A. Jr. Montgomery, J. E. Peralta, F. Ogliaro, M. Bearpark, J. J. Heyd, E. Brothers, K. N. Kudin, V. N. Staroverov, R. Kobayashi, J. Normand, K. Raghavachari, A. Rendell, J. C. Burant, S. S. Iyengar, J. Tomasi, M. Cossi, N. Rega, J. M. Millam, M. Klene, J. E. Knox, J. B. Cross, V. Bakken, C. Adamo, J. Jaramillo, R. Gomperts, R. E. Stratmann, O. Yazyev, A. J. Austin, R. Cammi, C. Pomelli, J. W. Ochterski, R. L. Martin, K. Morokuma, V. G. Zakrzewski, G. A. Voth, P. Salvador, J. J. Dannenberg, S. Dapprich, A. D. Daniels, O. Farkas, J. B. Foresman, J. V. Ortiz, J. Cioslowski and D. J. Fox, *Gaussian 09*, Gaussian, Inc., Wallingford, CT, 2010.
21 J. Zheng, S. Zhang, J. C. Corchado, R. Meana-Pañeda, Y. Y. Chuang, E. L. Coitiño, B. A. Ellingson and D. G. Truhlar, *GAUSSRATE 2016*, University of Minnesota, Minneapolis, 2016.
22 J. Zheng, J. L. Bao, R. Meana-Pañeda, S. Zhang, B. J. Lynch, J. C. Corchado, Y. Y. Chuang, P. L. Fast, W. P. Hu, Y. P. Liu, G. C. Lynch, K. A. Nguyen, C. F. Jackels, A. F. Ramos, B. A. Ellingson, V. S. Melissas, J. Villa, I. Rossi, E. L. Coitiño, J. Pu, T. V. Albu, A. Ratkiewicz, R. Steckler, B. C. Garret, A. D. Isaacson and D. G. Truhlar, *POLYRATE 2016*, University of Minnesota, Minneapolis, 2016.
23 J. C. Corchado, Y. Y. Chuang, P. L. Fast, W. P. Hu, Y. P. Liu, G. C. Lynch, K. A. Nguyen, C. F. Jackels, A. Fernandez-Ramos, B. A. Ellingson, B. J. Lynch, V. S. Melissas, J. Villá, I. Rossi, E. L. Coitinño, J. Pu, T. V. Albu, R. Steckler, B. C. Garrett, A. D. Isaacson and D. G. Truhlar, *POLYRATE 9.5*, University of Minnesota, Minneapolis, 2007.
24 J. Zheng, S. L. Mielke, K. L. Clarkson, R. Meana-Pañeda and D. G. Truhlar, *MSTor, version 2013*, University of Minnesota, Minneapolis, 2013.
25 J. Zheng, T. Yu, E. Papajak, I. M. Alecu, S. L. Mielke and D. G. Truhlar, *Phys. Chem. Chem. Phys.*, 2011, **13**, 10885–10907.
26 J. Zheng and D. G. Truhlar, *J. Chem. Theory Comput.*, 2013, **9**, 1356–1367.
27 T. Yu, J. Zheng and D. G. Truhlar, *Chem. Sci.*, 2011, **2**, 2199–2213.
28 NIST Computational Chemistry Comparison and Benchmark Database, NIST Standard Reference Database Number 101 2016, ed. D. Russell and III. Johnson, http://cccbdb.nist.gov/.
29 N. M. Donahue, G. T. Drozd, S. A. Epstein, A. A. Presto and J. H. Kroll, Adventures in Ozoneland: Down the Rabbit-hole, *Phys. Chem. Chem. Phys.*, 2011, **13**, 10848–10857.
30 M. Sipilä, T. Jokinen, T. Berndt, S. Richters, R. Makkonen, N. M. Donahue, R. L. Mauldin, T. Kurtén, P. Paasonen, N. Sarnela, M. Ehn, H. Junninen, M. P. Rissanen, J. Thornton, F. Stratmann, H. Herrmann, D. R. Worsnop, M. Kulmala, V. M. Kerminen and T. Petäjä, Reactivity of Stabilized Criegee Intermediates (sCIs) from Isoprene and Monoterpene Ozonolysis toward SO_2 and Organic Acids, *Atmos. Chem. Phys.*, 2014, **14**, 12143–12153.
31 K. Samanta, J. M. Beames, M. I. Lester and J. E. Subotnik, Quantum Dynamical Investigation of the Simplest Criegee Intermediate CH_2OO and its O–O Photodissociation Channels, *J. Chem. Phys.*, 2014, **141**, 134303.
32 Y. Zhao, N. E. Schultz and D. G. Truhlar, Design of Density Functionals by Combining the Method of Constraint Satisfaction with Parametrization for Thermochemistry, Thermochemical Kinetics, and Noncovalent Interactions, *J. Chem. Theory Comput.*, 2006, **2**, 364–382.
33 Y. Zhao and D. G. Truhlar, The M06 Suite of Density Functionals for Main Group Thermochemistry, Thermochemical Kinetics,

Noncovalent Interactions, Excited States, and Transition Elements: Two New Functionals and Systematic Testing of Four M06-class Functionals and 12 other Functionals, *Theor. Chem. Acc.*, 2008, **120**, 215–241.

34 M. Monge-Palacios and J. Espinosa-García, Reaction-Path Dynamics Calculations of the Cl + NH_3 Hydrogen Abstraction Reaction: The Role of the Intermediate Complexes, *J. Phys. Chem. A*, 2010, **114**, 4418–4426.

35 M. Monge-Palacios, C. Rangel, J. C. Corchado and J. Espinosa-García, Analytical Potential Energy Surface for the Reaction with Intermediate Complexes NH_3 + Cl → NH_2 + HCl: Application to the Kinetic Study, *Int. J. Quantum Chem.*, 2012, **112**, 1887–1903.

